Geochemical Perspectives Letters

Stable W isotope evidence for redistribution of homogeneous ^{182}W anomalies in SW Greenland

F. Kurzweil[1*], C. Münker[1], J.E. Hoffmann[2], J. Tusch[1], R. Schoenberg[3,4]

OPEN ACCESS

doi: 10.7185/geochemlet.2024

Abstract

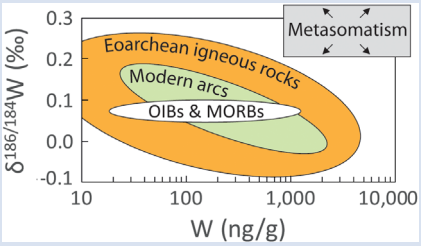

We present the first high precision stable tungsten isotope data for a comprehensive Eoarchean rock suite from the Isua region of SW Greenland with the aim to reconstruct the sources and processes that controlled the inventory of W in Eoarchean time and to place constraints on the origin of ^{182}W anomalies in Eoarchean rocks. When compared to modern igneous rocks, the observed range of $\delta^{186/184}$W in the Eoarchean rocks is substantially larger, ranging from −0.072 to +0.249 ‰. But unlike in modern igneous rocks, we find no co-variation of $\delta^{186/184}$W with other geochemical parameters. Multiple stage mobilisation and re-enrichment of W by metasomatic fluids entirely obscured pristine geochemical signals. However, our results illustrate the potential of applying stable W isotopes as geochemical tracer for alteration effects on primary ^{182}W signatures. Despite secondary alteration and the large variation in $\delta^{186/184}$W the excesses in ^{182}W that were previously observed in the same rock samples appear to be unaffected by alteration arguing that the excesses were most likely initially uniform in the whole Eoarchean assemblage of SW Greenland.

Received 16 January 2020 | Accepted 27 May 2020 | Published 15 July 2020

Introduction

The early Earth differed significantly from its present day geological setting. Higher potential mantle temperatures but lower heat fluxes (Korenaga, 2003) affected most relevant geological processes such as partial mantle melting with higher melt proportions, the mode of fractional crystallisation, and global tectonics (*e.g.*, de Wit *et al.*, 1992; Van Kranendonk, 2010). For example, it remains controversial if modern style plate tectonics operated on a global or local scale or were even absent in Hadean and Eoarchean times (*e.g.*, de Wit *et al.*, 1992; Nutman *et al.*, 1996; Van Kranendonk, 2010). Alternative models suggest vertical stagnant lid tectonics, where thickened and dense eclogitic crustal restites sink in sagduction regimes (*e.g.*, Bédard, 2006). In the latter case, crustal recycling would have differed, also affecting the geochemical cycling of elements and thus, the geochemical composition of early crustal nuclei.

Stable W isotopes represent an emerging geochemical tool that might help to reconstruct the geologic and tectonic history of ancient rocks as well as the cycling of W through different geochemical reservoirs (Kurzweil *et al.*, 2019; Mazza *et al.*, 2020). Distinct types of modern igneous rocks show resolvable variation in the stable W isotope compositions. For example, subduction related rocks that carry a significant subducted sediment component show isotopically heavy compositions for W. In contrast, isotopically lighter compositions were observed in back-arc lavas that formed above deeper subduction zone settings, more distant to the trench (Mazza *et al.*, 2020). Fractional crystallisation of olivine and pyroxene as well as partial melting of mantle peridotite, however, have limited and so far not resolvable effects on the stable W isotope composition of mafic and intermediate melts. Accordingly, plume related rocks from ocean island basalt settings and mid-ocean ridge basalts show limited variation in $\delta^{186/184}$W values (Eq. S-1), calling for a homogeneous modern mantle stable W isotope composition of +0.085 ± 0.019 ‰. (Fig. 1; Kurzweil *et al.*, 2019; Mazza *et al.*, 2020).

In this study, we present stable W isotope data for some of the Earth's oldest rocks from the Itsaq Gneiss Complex, SW Greenland (IGC, 3620 to >3850 Ma; *e.g.*, Nutman *et al.*, 1996) including peridotites, tholeiitic metabasalts, boninite-like metabasalts, non-gneissic tonalite-trondhjemite-granodiorites (TTGs) and metasediments, with the aim to reconstruct the sources and processes that controlled the inventory of W in Eoarchean time. This region is of particular interest, because of widespread metasomatic alteration (Rosing *et al.*, 1996) and a previously reported large scale mobility of W (Rizo *et al.*, 2016; Tusch *et al.*, 2019) that even led to ore grade enrichment of W at a local scale (Appel, 1986). Moreover, the IGC is one of the first localities on Earth, where significant ^{182}W excesses were reported (*e.g.*, Willbold *et al.*, 2011; the excess of ^{182}W is described by μ^{182}W, which is defined in the SI), and stable W isotopes may aid to elucidate the significance of these isotope anomalies. We combine the stable W isotope data with previously published major and trace element concentration data

1. Institut für Geologie und Mineralogie, Universität zu Köln, Zülpicher Str. 49b, 50674 Köln, Germany
2. Institut für Geologische Wissenschaften, Freie Universität Berlin, Malteserstr. 74-100, 12249 Berlin, Germany
3. Department of Geosciences, Eberhard Karls University Tübingen, Wilhelmstr. 56 72074 Tübingen, Germany
4. Department of Geology, University of Johannesburg, P.O. Box 524, Auckland Park 2006, South Africa
* Corresponding author (email: flokurzweil@hotmail.de)

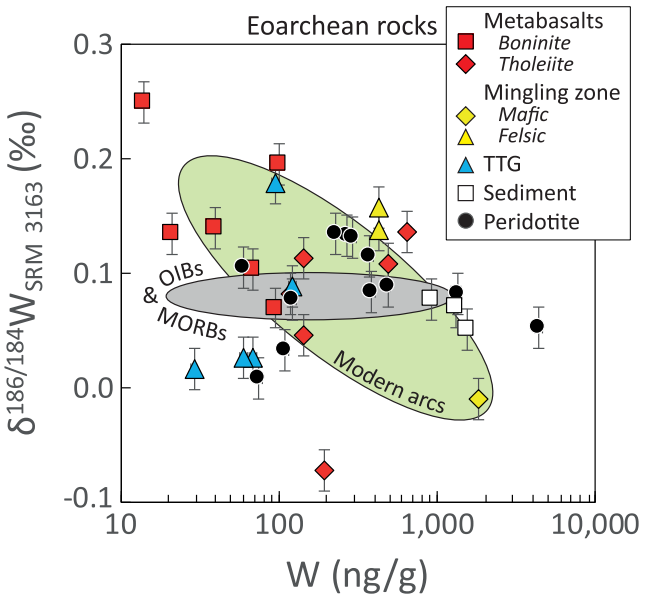

Figure 1 Plot of stable W isotope compositions and W concentrations for Eoarchean rocks from the Itsaq Gneiss Complex. The observed range in $\delta^{186/184}$W is even larger when compared to samples from modern OIBs, MORBs and arcs, and the variations are probably related to stable W isotope fractionation during local metasomatic processes.

as well as with μ^{182}W data obtained for the same set of samples (Tusch *et al.*, 2019) to place constraints on the geodynamic setting of the magmatic rocks, their relationship among each other and possible hydrothermal and metasomatic overprint.

Results

A detailed description of the sample material, the geological setting and the analytical procedure can be found in the SI. The peridotite samples show extreme variations in W concentrations between 59 and 4380 ng/g, corresponding to W/Th between 0.02 and 143. Their stable W isotope compositions range from +0.008 to +0.134 ‰ in $\delta^{186/184}$W (Table S-1, Fig. 1). Tholeiitic metabasalts show similarly variable W concentrations between 117 and 1835 ng/g (W/Th from 0.2 to 2.3) and an even larger range in $\delta^{186/184}$W (−0.072 to +0.136 ‰), clearly outside the range predicted for igneous processes (Kurzweil *et al.*, 2019; Mazza *et al.*, 2020). In contrast, the boninite-like metabasalts are more depleted in W with concentrations between 14 and 100 ng/g. These rocks show elevated $\delta^{186/184}$W values between +0.069 and +0.249 ‰. Non-gneissic TTGs range in W concentrations between 29 and 430 ng/g (W/Th between 0.01 and 0.35). The stable W isotope compositions vary between +0.016 and +0.179 ‰ in $\delta^{186/184}$W, thus showing a similar range as most mafic and ultramafic rocks (Table S-1, Fig. 1). In contrast, metasediments that are relatively rich in W (928 to 1547 ng/g) exhibit a smaller range in $\delta^{186/184}$W between +0.050 and +0.077 ‰.

In the complete dataset we observe no clear co-variation of $\delta^{186/184}$W values with any other geochemical parameters (Fig. 2), neither with major or trace element concentrations nor with element concentration ratios. The variability in $\delta^{186/184}$W values is independent of the geographic position, the age, and the rock type of the sample. Similarly, W concentrations show no co-variation with other element concentrations or with element concentration ratios (Fig. S-1).

Discussion

The major and trace element composition of tholeiitic and boninite-like metabasalts from the IGC is mainly controlled by fractional crystallisation of olivine and pyroxene (Polat and Hofmann, 2003), whereby the boninite-like melts originate from an already depleted, more harzburgitic mantle source. The peridotites of this study represent relict mantle rocks (van de Löcht *et al.*, 2018), and the TTGs likely formed by partial melting of hydrated mafic crust (*e.g.*, Hoffmann *et al.*, 2014; SI). The close genetic relationship of the rock suites analysed here might explain the observed tight co-variations between various compatible and incompatible elements (Table S-2, Fig. S-1; Tusch *et al.*, 2019). Most elements that behave incompatibly during partial melting and fractional crystallisation of olivine and pyroxene (Zr, Th, Ba, Pb) show expected enrichments in more

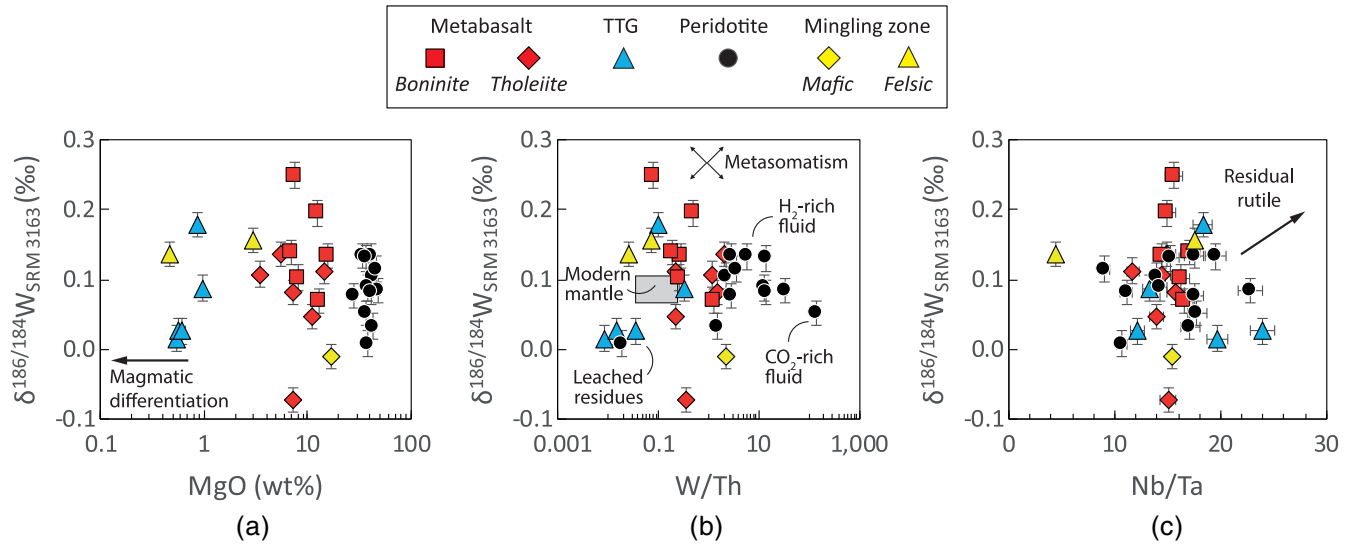

Figure 2 Plots of measured W isotope compositions **(a)** *versus* MgO as an indicator for magmatic differentiation, **(b)** *versus* W/Th as an indicator for selective W mobility by metasomatic fluids and **(c)** *versus* Nb/Ta as an indicator for the presence of residual rutile during partial melting. We observe no co-variation of $\delta^{186/184}$W values neither with any element concentration nor with any element ratio.

differentiated rocks, whereas compatible elements such as Mg, Ni and Co are more depleted (Fig. S-1). These differentiation trends are even preserved for some fluid mobile elements (Ba, Pb), which is noteworthy, considering the complex geologic history of igneous rocks from the IGC that experienced several high grade metamorphic, hydrothermal and metasomatic events (Nutman *et al.*, 1996; Rosing *et al.*, 1996). Partial recrystallisation during amphibolite facies grade metamorphism (*e.g.*, the formation of secondary amphibole, feldspar and biotite) apparently changed the mineralogy without significantly changing the overall bulk geochemical composition for most elements. However, the incompatible and fluid mobile element W shows no co-variation with any other element (Fig. S-1), indicating that its budget was severely affected during metamorphism, metasomatism and hydrothermalism. Extreme W concentrations in peridotites up to 4380 ng/g (more than 100 fold compared to 12 ng/g of the modern mantle; König *et al.*, 2011) and W/Th (0.02–143) that are, with the exception of sample 10–12A, highly elevated compared to the canonical value defined by modern igneous rocks and clearly indicate secondary enrichment of W (Rizo *et al.*, 2016; Tusch *et al.*, 2019). Primary hosts for secondary W enrichments by metasomatic fluids are minor mineral phases such as serpentine, Ti-rich mineral phases, phlogopite and sulfide or grain boundary assemblages (Liu *et al.*, 2018). Indeed, fine serpentine veinlets as well as small metasomatic sulfides have been reported for most peridotites investigated here (van de Löcht *et al.*, 2018, 2020). Consistent with a previous study (Rizo *et al.*, 2016), we thus suggest that W was strongly mobilised by metasomatic fluids. This secondary disturbance of W probably increased the variation in $\delta^{186/184}$W beyond the range that is expected for unaltered igneous rocks (Kurzweil *et al.*, 2019; Mazza *et al.*, 2020). Therefore, our data provides no straightforward insight into tectono-magmatic processes active during the formation of the IGC.

The chemical composition of metasomatic fluids in the Isua region was shown to be variable on local to regional scales depending on the ambient rock assemblage (Rosing *et al.*, 1996). This local heterogeneity probably also accounts for heterogeneous W concentrations and stable W isotope compositions of the ambient fluids and for the decoupling of W that is typically dissolved as an oxyanion, which can be complexed with cationic ligands such as K^+ or H^+, from other nominally fluid mobile elements such as Ba or Pb that are transported as metal cations, which are complexed with anionic ligands such as Cl^- (Wood and Samson, 2000). The observed variability in $\delta^{186/184}$W values, which is not correlated with W concentrations (Fig. 1), argues against a single, regionally homogeneous metasomatising fluid that overprinted primary stable W isotope compositions of IGC rocks to the same extent. The large variation of $\delta^{186/184}$W within different rock types rather calls for the involvement of different metasomatic fluids with locally (and temporally) variable stable W isotope compositions. To explain this local and temporal variability in $\delta^{186/184}$W, stable W isotope fractionation at various geologic conditions is required.

In general, the magnitude of equilibrium isotope fractionation in geological environments depends on differences in bond strengths, whereby heavy isotopes prefer stronger bonding environments such as high oxidation states and low coordination numbers. Stable W isotope fractionation caused by redox changes in terrestrial igneous environments is not expected (Kurzweil *et al.*, 2019), because the oxidised W^{6+} species is predominant in these settings (Fonseca *et al.*, 2014). However, during metasomatic alteration the preferential leaching of isotopically heavy W, which is mainly abundant as a tetrahedrally coordinated anion $[WO_4]^{2-}$ in fluids, is expected, similar as in modern fluid-dominated subduction zone settings (Mazza *et al.*, 2020). Moreover, octahedral coordination is preferred in hexagonally close packed mineral structures (*e.g.*, wolframite), whereas the complex remains in tetrahedral coordination in cubic closed packed minerals (*e.g.*. scheelite; Kuzmin and Purans, 2001). As such W-rich minerals are reported in the IGC (Appel, 1986), we speculate that the local remobilisation of W by metasomatic and hydrothermal fluids (and possibly seawater) as well as the formation of secondary W-rich mineral phases caused mass dependent stable W isotope fractionation in different directions due to localised changes in coordination.

To understand the metasomatic processes in more detail the separate consideration of distinct rock types and their specific petrographic properties is necessary. For example, TTGs with sub-canonical W/Th show low $\delta^{186/184}$W, whereas TTGs with canonical or supra-canonical W/Th show higher $\delta^{186/184}$W (Fig. 2b). A similar relationship is observed for peridotites. Most peridotite samples show strong W enrichment (high W/Th) and relatively high $\delta^{186/184}$W. The only peridotite with sub-canonical W/Th was also hydrated most strongly (10–12A; van de Löcht *et al.*, 2020) and shows the lowest $\delta^{186/184}$W of all peridotites. These relationships indicate the preferential mobilisation of isotopically heavy W by metasomatic fluids, leaving behind W depleted rocks that are isotopically lighter (Fig. 2b). The apparently higher number of W-rich peridotites with high $\delta^{186/184}$W might reflect sampling bias, as strongly altered samples such as 10–12A are usually excluded. Thus, strong W enrichments in peridotites do not necessarily require external sources of W but could also relate to very local W redistribution within single rock types. Importantly, W-rich peridotites in SW Greenland were metasomatised by chemically different fluids (H_2-rich *vs.* CO_2-rich; Rosing *et al.*, 1996) as also indicated by crosscutting fine serpentine veins (SOISB1 and NUB peridotites) and carbonate veins (sample 10–34), respectively (van de Löcht *et al.*, 2020). Generally high W/Th in these samples indicate that both fluids were rich in W but it seems that W concentrations were higher and $\delta^{186/184}$W slightly lower in CO_2-rich fluids that percolated the carbonate bearing peridotite 10–34 (Fig. 2b). These relationships clearly suggest that the source of W in metasomatic fluids was heterogeneous and of different isotopic polarity.

Compared to modern igneous rocks, samples from the IGC show uniform excesses in the radiogenic isotope ^{182}W. This excess was explained by either a missing late veneer component that was depleted in ^{182}W (Willbold *et al.*, 2011; Dale *et al.*, 2017), or by early silicate differentiation during the lifetime of short lived ^{182}Hf and the respective formation of ^{182}W-enriched and ^{182}W-depleted silicate reservoirs, respectively (Rizo *et al.*, 2016; Tusch *et al.*, 2019). In all these studies, mass dependent isotope fractionation that occurred during the chemical separation of W and the measurement of W isotope abundances is corrected assuming the exponential mass fractionation law and a given reference value of the ^{186}W/^{184}W ratio. However, natural mass dependent isotope fractionation during fluid controlled processes might have followed a different mass fractionation law (*e.g.*, Hart and Zindler, 1989; SI). The application of inappropriate mass fractionation laws may therefore theoretically create apparent mass independent isotope effects in μ^{182}W (Hart and Zindler, 1989; SI). Assuming the equilibrium mass fractionation law during natural stable W isotope fractionation, however, the observed range in $\delta^{186/184}$W can maximally account for ^{182}W excesses that are smaller than 2 ppm in μ^{182}W (Fig. S-2, Table S-3) a similar range that was also previously predicted by stable W isotope data of lower precision (Rizo *et al.*, 2016). Moreover, we observe no co-variation of μ^{182}W and $\delta^{186/184}$W values (Fig. 3). Thus, ^{182}W excesses of around

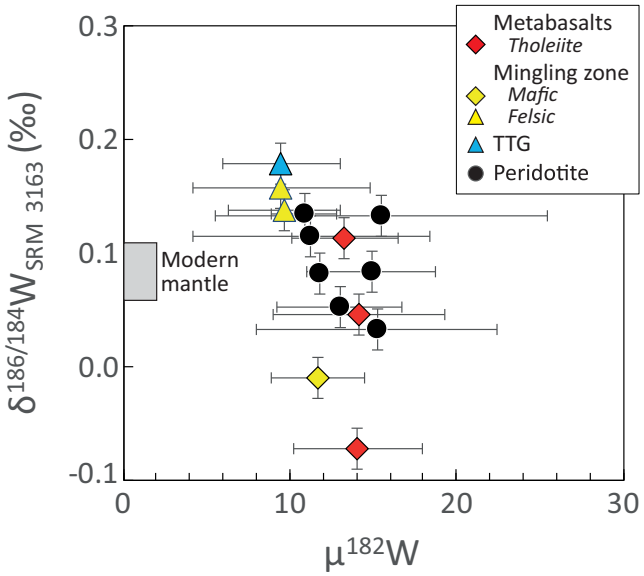

Figure 3 Despite variable $\delta^{186/184}W$, the excess of ^{182}W is homogeneously distributed in igneous rocks from the IGC (Tusch *et al.*, 2019). We hypothesise that mass dependent stable W isotope fractionation during multi-stage metasomatic redistribution of W caused locally variable $\delta^{186/184}W$ without affecting the regionally homogeneous mass independent excesses of ^{182}W.

+13 ppm in rocks of the IGC (Willbold *et al.*, 2011; Rizo *et al.*, 2016; Dale *et al.*, 2017; Tusch *et al.*, 2019) represent no analytical artefacts caused by the application of inappropriate mass fractionation laws.

Despite variable secondary enrichment of W and heterogeneous $\delta^{186/184}W$ beyond the range observed in fresh igneous rocks, the excess of ^{182}W is homogeneously distributed in igneous rocks from the IGC (Tusch *et al.*, 2019). We therefore suggest that mass dependent stable W isotope fractionation during multi-stage metasomatic redistribution of W increased the variability in $\delta^{186/184}W$ on a local scale without affecting the mass independent excesses of ^{182}W. The sources of the metasomatic W likely tap different rock types as indicated by extremely variable W/Th and $\delta^{186/184}W$ in all analysed rock types. These observations argue against initially variable excesses in ^{182}W that were fully homogenised but are more consistent with an originally widespread and homogeneously distributed excess of ^{182}W within the Eoarchean assemblage of the IGC prior to the metasomatic redistribution of W. From a W perspective, this would permit combination with other geochemical parameters such as ^{142}Nd isotope or HSE signatures (*e.g.*, Rizo *et al.*, 2016; Dale *et al.*, 2017; Saji *et al.*, 2018). In the light of coupled ^{182}W-^{142}Nd anomalies (Rizo *et al.*, 2016) and recently reported Ru isotope data (Fischer-Gödde *et al.*, 2020), contributions from both missing late veneer and early silicate differentiation to the ^{182}W excesses now appear likely. For future ^{182}W isotope studies, the combination with stable W isotope analyses might represent an additional tool to assess the pristine character of W signatures.

Acknowledgements

This study is part of the "Infant Earth" project that has received funding from the European Research Council (ERC) under the European Union's Horizon 2020 research and innovation programme (grant agreement No 669666). We thank Austin Boyd and Minik Rosing for providing sample material. Helen Williams is acknowledged for editorial handling. Constructive comments raised by two anonymous reviewers and Helen Williams helped to improve the quality of the article.

Editor: Helen Williams

Additional Information

Supplementary Information accompanies this letter at http://www.geochemicalperspectivesletters.org/article2024.

Cite this letter as: Kurzweil, F., Münker, C., Hoffmann, J.E., Tusch, J., Schoenberg, R. (2020) Stable W isotope evidence for redistribution of homogeneous ^{182}W anomalies in SW Greenland. *Geochem. Persp. Let.* 14, 53–57.

References

Appel, P.U. (1986) Strata bound scheelite in the Archean Malene supracrustal belt, West Greenland. *Mineralium Deposita* 21, 207–215.

Bédard, J.H. (2006) A catalytic delamination-driven model for coupled genesis of Archaean crust and sub-continental lithospheric mantle. *Geochimica et Cosmochimica Acta* 70, 1188–1214.

Dale, C.W., Kruijer, T.S., Burton K.W. (2017) Highly siderophile element and 182W evidence for a partial late veneer in the source of 3.8 Ga rocks from Isua, Greenland. *Earth and Planetary Science Letters* 458, 394–404.

Fischer-Gödde, M., Elfers, B.-M., Münker, C., Szilas, K., Maier, W.D., Messling, N., Morishita, T., Van Kranendonk, M., Smithies, H. (2020) Ruthenium isotope vestige of Earth's pre-late-veneer mantle preserved in Archaean rocks. *Nature* 579, 240–244.

Fonseca, R.O.C., Mallmann, G., Sprung, P., Sommer, J.E., Heuser, A., Speelmanns, I.M., Blanchard, H. (2014) Redox controls on tungsten and uranium crystal/silicate melt partitioning and implications for the U/W and Th/W ratio of the lunar mantle. *Earth and Planetary Science Letters* 404, 1–13.

Hart, S.R., Zindler, A. (1989) Isotope fractionation laws. *International Journal of Mass Spectrometry and Ion Processes* 89, 287–301.

Hoffmann, J.E., Nagel, T.J., Muenker, C., Næraa, T., Rosing, M.T. (2014) Constraining the process of Eoarchean TTG formation in the Itsaq Gneiss Complex, southern West Greenland. *Earth and Planetary Science Letters* 388, 374–386.

König, S., Münker, C., Hohl, S., Paulick, H., Barth, A.R., Lagos, M., Pfänder, J., Büchl, A. (2011) The Earth's tungsten budget during mantle melting and crust formation. *Geochimica et Cosmochimica Acta* 75, 2119–2136.

Korenaga, J. (2003) Energetics of mantle convection and the fate of fossil heat. *Geophysical Research Letters* 30.

Kurzweil, F., Münker, C., Grupp, M., Braukmüller, N., Fechtner, L., Christian, M., Hohl, S.V., Schoenberg, R. (2019) The stable tungsten isotope composition of modern igneous reservoirs. *Geochimica et Cosmochimica Acta* 251, 176–191.

Kuzmin, A., Purans, J. (2001) Local atomic and electronic structure of tungsten ions in AWO4 crystals of scheelite and wolframite types. *Radiation measurements* 33, 583–586.

Liu, J., Pearson, D.G., Chacko, T., Luo, Y. (2018) A reconnaissance view of tungsten reservoirs in some crustal and mantle rocks: Implications for interpreting W isotopic compositions and crust-mantle W cycling. *Geochimica et Cosmochimica Acta* 223, 300–318.

Mazza, S.E., Stracke, A., Gill, J.B., Kimura, J.-I., Kleine, T. (2020) Tracing dehydration and melting of the subducted slab with tungsten isotopes in arc lavas. *Earth and Planetary Science Letters* 530, 115942.

Nutman, A.P., McGregor, V.R., Friend, C.R.L., Bennett, V.C., Kinny, P.D. (1996) The Itsaq gneiss complex of southern West Greenland; the world's most extensive record of early crustal evolution (3900-3600 Ma). *Precambrian Research* 78, 1–39.

Polat, A., Hofmann, A.W. (2003) Alteration and geochemical patterns in the 3.7–3.8 Ga Isua greenstone belt, West Greenland. *Precambrian Research* 126, 197–218.

Rizo, H., Walker, R.J., Carlson, R.W., Touboul, M., Horan, M.F., Puchtel, I.S., Boyet, M., Rosing, M.T. (2016) Early Earth differentiation investigated through 142Nd, 182W, and highly siderophile element abundances in samples from Isua, Greenland. *Geochimica et Cosmochimica Acta* 175, 319–336.

Rosing, M.T., Rose, N.M., Bridgwater, D., Thomsen, H.S. (1996) Earliest part of Earth's stratigraphic record. *Geology* 24, 43–46.

Saji, N.S., Larsen, K., Wielandt, D., Schiller, M., Costa, M.M., Whitehouse, M.J., Rosing, M.T., Bizzarro, M. (2018) Hadean geodynamics inferred from time-varying 142Nd/144Nd in the early Earth rock record. *Geochemical Perspectives Letters* 7, 43–48.

Tusch, J., Sprung, P., van de Löcht, J., Hoffmann, J.E., Boyd, A.J., Rosing, M.T., Münker, C. (2019) Uniform 182W isotope compositions in Eoarchean rocks from the Isua region, SW Greenland. *Geochimica et Cosmochimica Acta* 257, 284–310.

van de Löcht, J., Hoffmann, J.E., Li, C., Wang, Z., Becker, H., Rosing, M.T., Kleinschrodt, R., Münker, C. (2018) Earth's oldest mantle peridotites show entire record of late accretion. *Geology* 46, 199–202.

van de Löcht, J., Hoffmann, J.E., Rosing, M.T., Sprung, P., Münker, C. (2020) Preservation of Eoarchean mantle processes in ~3.8 Ga peridotite enclaves in the Itsaq Gneiss Complex, southern West Greenland. *Geochimica et Cosmochimica Acta* 280,1–25.

Van Kranendonk, M.J. (2010) Two types of Archean continental crust. *American Journal of Science* 310, 1187–1209.

Willbold, M., Elliott, T., Moorbath, S. (2011) The tungsten isotopic composition of the Earth's mantle before the terminal bombardment. *Nature* 477, 195.

de Wit, M.J., de Ronde, C.E.J., Tredoux, M., Roering, C., Hart, R.J., Armstrong, R.A., Green, R.W.E., Peberdy, E., Hart, R.A. (1992) Formation of an Archaean continent. *Nature* 357, 553.

Wood, S.A., Samson, I.M. (2000) The hydrothermal geochemistry of tungsten in granitoid environments. *Economic Geology* 95, 143–182.

Geochemical Perspectives Letters

Stable W isotope evidence for redistribution of homogeneous ^{182}W anomalies in SW Greenland

F. Kurzweil, C. Münker, J.E. Hoffmann, J. Tusch, R. Schoenberg

Supplementary Information

The Supplementary Information includes:

- Geological Setting and Sample Material
- Methods, Analytical Precision and Accuracy
- The Influence of Different Mass Fractionation Laws on $\mu^{182}W$
- Figures S-1 and S-2
- Tables S-1 to S-3
- Supplementary Information References

Geological Setting and Sample Material

The Itsaq Gneiss Complex (IGC) in SW Greenland consists of up to 80 % of granitoids of the tonalite, trondhjemite-granodiorite (TTG) suite associated with complex assemblages of amphibolites, chemical and clastic sediments as well as felsic- to ultramafic units. (Moorbath *et al.*, 1973; Nutman *et al.*, 1996). Based on separate metamorphic histories it is subdivided into the Isukasia terrane (ISB and SOISB samples, Table S-1) and the Færingehavn terrane (NUK samples, Table S-1; Nutman *et al.*, 1996). Part of the Isukasia terrane is the Isua supracrustal belt (ISB), which is further divided into a 3.7 Ga old northern terrane and a 3.8 Ga old southern terrane (Nutman and Friend, 2009). Supracrustal rock assemblages and metatonalitic orthogneisses from the Northern- and Southern terrane are crosscut by the ~3.45-3.55 Ga old noritic Ameralik dykes. Juxtaposition of both terranes was dated to 3.68 Ga on a sedimentary mylonitic unit that separates both terranes (Nutman and Friend, 2009). Most rocks of the IGC were metamorphosed to amphibolite grade during at least two major metamorphic events at 3.61 Ga and 3.55 Ga (Blichert-Toft and Frei, 2001; Nutman *et al.*, 2002; Crowley, 2003). Furthermore, the IGC region experienced several phases of metasomatic alteration by fluids of locally variable composition (carbonate- and H_2O-rich; Rose *et al.*, 1996; Rosing *et al.*, 1996). The stage of deformation also varies locally including high- and low strain domains (Nutman *et al.*, 1996; Nutman and Friend, 2009).

Supracrustal rock assemblages of the IGC mainly consist of amphibolites with island arc tholeiitic geochemical affinity (herein called tholeiitic metabasalts; Polat *et al.*, 2002; Jenner *et al.*, 2009; Nutman and Friend, 2009; Hoffmann *et al.*, 2010). In the ISB typical pillow structures are locally preserved indicating low grades of deformation (Nutman and Friend, 2009). Abundant quartz globules and quartz veins contain unstrained quartz that pre-dates metamorphic fabrics. These globules and veins were interpreted to reflect chemical precipitates from circulating ocean-floor-type hydrothermal fluids (Appel *et al.*, 2001). The Northern terrane of the ISB also includes amphibolites with boninitic character that are petrogenetically unrelated to amphibolites with island arc tholeiitic affinity (Polat *et al.*, 2002; Polat and Hofmann, 2003). In contrast to the tholeiitic basalts, the boninite-like metabasalts formed by partial melting of a depleted harzburgitic mantle source, which was poor in clinopyroxene due to its progressive extraction during earlier melting events (Green, 1976; Tatsumi, 1989; van der Laan *et al.*, 1989). Boninite-like metabasalts of this study originate from the

eastern limb of the Isua Greenstone belt. Their original mineralogical composition was replaced during metamorphism by amphibole, plagioclase, chlorite, epidote, titanite and quartz (Polat *et al.*, 2002). A more detailed description of tholeiitic and boninite-like metabasalts that have been analysed for this study can be found in Polat *et al.* (2002), Hoffmann *et al.* (2010) and Tusch *et al.* (2019). In the western part of the ISB a mingling association of felsic and mafic magma was recently discovered (Boyd, 2018). The mafic unit is of tholeiitic composition. The felsic magma derived from partial melting of gabbro, which was previously altered by hydrothermal fluids (Boyd, 2018). The felsic unit shows a petrogenetic relationship to the massive felsic unit in the centre of the ISB thus not representing a late addition to the ISB (Boyd, 2018). The mingling association preserved primary magmatic structures that rather indicate the coeval eruption of felsic and mafic units, which was dated to 3808.0 ± 1.2 Ma (Boyd, 2018). Samples analysed for this study include a granular felsic rock, as well as a mafic and a leucosome enclave close to the mafic felsic contact. A more detailed description of this association can be found in Boyd (2018) and Tusch *et al.* (2019).

Metatonalitic orthogneisses and non-gneissic TTGs from the IGC represent some of the oldest fragments of continental crust (Nutman *et al.*, 1999). They formed either by melting of subducted mafic crust at high pressures (Defant and Drummond, 1990; Rapp *et al.*, 2003) or by melting of thickened island-arc crust at relatively lower pressures (Smithies, 2000; Hoffmann *et al.*, 2011; Nagel *et al.*, 2012). These felsic melts likely originated from partial melting of above mentioned tholeiites (Hoffmann *et al.*, 2011, 2014). TTGs intruded slightly older ultramafic supracrustal rock assemblages that were already deformed and metamorphosed prior to the intrusion (Nutman and Friend, 2009; Hoffmann *et al.*, 2011). Within this study non-gneissic TTGs from the ISB and a low strain area south of the ISB were also analysed. These samples consist of plagioclase, quartz, hornblende, biotite, apatite and titanite. More details can be found in Hoffmann *et al.* (2014).

The area south of the ISB also comprises ultramafic lenses that are tectonically intercalated in tonalitic gneisses and TTGs (Nutman *et al.*, 1996). In contrast to supracrustal amphibolites, these dunitic and harzburgitic enclaves might either reflect their derivative cumulates (Szilas *et al.*, 2015) or relicts of Eoarchean mantle rocks (*e.g.* van de Löcht *et al.*, 2018, 2020). Szilas *et al.* (2015) observed ultramafic units in the ISB further to the north with olivine crystals that are enclosed by serpentine. These authors interpreted the olivine to be of metamorphic origin that formed during dehydration of serpentinized rocks. The ultramafic rocks from south of the ISB analysed for this study contain olivine, orthopyroxene and amphibole with minor amounts of serpentine, biotite, chlorite and sulphides, the latter minerals being mainly linked to small veinlets (van de Löcht *et al.*, 2018, 2020). Despite the limited stability of olivine at hydrous low pressure conditions, mantle-like PGE patterns and the chemical composition of the olivines both indicate that these ultramafic units reflect mantle residues instead of cumulates (van de Löcht *et al.*, 2018). A more detailed description of our ultramafic samples can be found in Friend *et al.* (2002), van de Löcht *et al.* (2018) and Tusch *et al.* (2019).

The sediment unit that separates the Northern and the Southern terrane of the ISB mainly consists of metamorphosed and metasomatized cherts, siliciclastic turbidites, carbonates and banded iron formations. Metasediments analysed for this study are from the Garbenschiefer Formation in the western limb of the ISB having an approximate age of 3.72 Ga (Rosing, 1999; Kamber *et al.*, 1998). The mineralogical composition of these sediments comprises quartz, mica, chlorite, chalcopyrite and graphite (more details in Rosing, 1999 and Hoffmann *et al.*, 2010).

Methods, Analytical Precision and Accuracy

Short summaries of the chemical separation procedure and measurement parameters are presented in Tables S-3 and S-4. The stable W isotope composition of pure W cuts was measured using a ThermoFisher Scientific® NeptunePlus MC-ICP-MS at the University of Cologne. Details of the measurement setup parameters are provided in Kurzweil *et al.*, (2018). The iterative solution of Compston and Oversby (1969) was applied for the data reduction of individual measurement cycles assuming that the instrumental mass bias follows the exponential law. To correct for the isobaric interferences of $^{180}Hf^+$,$^{180}Ta^+$,$^{184}Os^+$, and $^{186}Os^+$ we simultaneously measured $^{177}Hf^+$,$^{181}Ta^+$ and $^{188}Os^+$ and assumed the same instrumental mass bias for these elements as for W. We present our data in the δ-notation and relative to NIST SRM 3163 in ‰:

$$\delta^{186/184}\mathrm{W} = \left(\frac{\left(\frac{^{186}W}{^{184}W}\right)_{\mathrm{Sample}}}{\left(\frac{^{186}W}{^{184}W}\right)_{\mathrm{NIST\ SRM\ 3163}}} - 1 \right) x\ 1000 \qquad \text{Eq. S-1}$$

The standard NIST SRM 3163 as well as an Alfa Aesar reference solution were repeatedly measured during measurement sequences having a long-term reproducibility in $\delta^{186/184}W$ of 0.000 ± 0.012 ‰ (n = 148) and +0.055 ± 0.016 ‰ (n = 113), respectively. Between different measurement sessions (n = 13), the average isotopic difference between Alfa Aesar and NIST SRM 3163 was very constant with $\Delta^{186/184}W$ = 0.056 ± 0.010 ‰. Additionally, the reference materials AGV-2 and BCR-2 were measured repeatedly, also including individual processing through the complete chemical separation procedure. Results for the andesitic reference material

AGV-2 (+0.007 ± 0.013 ‰; 2 s.d.; n = 6) and the basalt BCR-2 (+0.064 ± 0.006 ‰; 2 s.d.; n = 5) are consistent with previously determined compositions (Krabbe *et al.*, 2016; Kurzweil *et al.*, 2018) and confirm the previously reported 2 SD external reproducibility of ±0.018 ‰ in $\delta^{186/184}W$.

The Influence of Different Mass Fractionation Laws on $\mu^{182}W$

Mass fractionation laws relate a mass dependent isotope fractionation that is observed for one isotope ratio R_A with $R_A = N_2/N_1$ to a second isotope ratio R_B of the same element with $R_B = N_3/N_1$, where N_i is the abundance of isotope i with mass m_i. This relation can be expressed by the isotope fractionation factor $\alpha_A = \alpha_B^{\beta}$. The exponent β is a function of the masses of the isotopes and can be calculated using different mass fractionation laws (Wombacher *et al.*, 2003). For example:

Equilibrium law	$\beta = (1/m_1 - 1/m_2) / (1/m_1 - 1/m_3)$	(Young *et al.*, 2002)	Eq. S-2
Exponential (Kinetic) law	$\beta = \ln(m_1/m_2) / \ln(m_1/m_3)$	(Young *et al.*, 2002)	Eq. S-3
Power law	$\beta = (m_1 - m_2) / (m_1 - m_3)$	(Maréchal *et al.*, 1999)	Eq. S-4

The exponential and the power law represent empirical relationships to describe the instrumental mass bias during isotope measurements (Russel *et al.*, 1978; Hart and Zindler, 1989; Maréchal *et al.*, 1999). The equilibrium and the kinetic law describe theoretical considerations that follow equilibrium isotope exchange and kinetic isotope fractionation processes, respectively (Young *et al.*, 2002). In most W isotope studies mass dependent isotope fractionation that occurred during the measurement of W isotope abundances is corrected assuming the exponential mass fractionation law using a given reference value of $^{186}W/^{184}W = 0.927670$ (Völkening *et al.*, 1991). However, stable W isotope fractionation during the chemical separation of W and metasomatic alteration prior to the separation and measurement of W isotopes might be better described by another mass fractionation law such as the equilibrium law. The inappropriate application of mass fractionation laws can create apparent anomalies in single isotope abundancies (Hart and Zindle, 1989; Rizo *et al.*, 2016), an effect that will be described in more detail below.

Relative to a standard the isotope ratios R_A and R_B are expressed as δ-values with $\delta_{A\ sample} = (R_{A\ sample} / R_{A\ Std} - 1) \times 1000$ and $\delta_{B\ sample} = (R_{B\ sample} / R_{B\ Std} - 1) \times 1000$. Assuming no mass independent isotope fractionation, δ_A and δ_B are related by $\delta_B = 1000 \times [(1 + \delta_A / 1000)^{\beta} - 1)]$ (*e.g.* Farquhar *et al.*, 2002). The larger the difference in δ_A (which is calculated as difference to an unfractionated modern mantle $\delta^{186/184}W$ value of +0.085 ‰ with $\delta_A = \delta_{A\ sample} - \delta_{A\ modern\ mantle}$ Kurzweil *et al.*, 2019), the larger is the difference between δ_B that is calculated using the exponential law and δ_B that is calculated using the equilibrium law. Accordingly, R_B ratios are also slightly different, which results in relative excesses/depletions of the isotope N_3. This excess/depletion can be estimated by $\mu^{N3} = (R_B\ law_1 / R_B\ law_2 - 1) \times 10^6$. For example, for $N_1 = {}^{184}W$, $N_2 = {}^{186}W$, $N_3 = {}^{182}W$ we get $R_A = {}^{186}W/{}^{184}W$ and $R_B = {}^{182}W/{}^{184}W$. Relative to the modern upper mantle, samples from the IGC show a maximum in $\delta^{186/184}W$ of +0.164 ‰ and a minimum in $\delta^{186/184}W$ of -0.157 ‰, respectively. Using the β value of the equilibrium law (law1) and the exponential law (law2) and a $^{182}W/^{184}W$ ratio of 0.864780 (Völkening *et al.*, 1991), the $\mu^{182}W_{Equilibrium}$ is then -1.8 ppm for the maximum $\delta^{186/184}W$ value and +1.7 ppm for the minimum $\delta^{186/184}W$ value (Fig. S-2; Table S-3). Using the β value of the power law (law1) and the exponential law (law2), the $\mu^{182}W_{Power}$ is +1.8 ppm for the maximum $\delta^{186/184}W$ value and -1.7 ppm for the minimum $\delta^{186/184}W$ value (Fig. S-2; Table S-3). Thus, the application of different mass fractionation laws can theoretically only account for apparent excesses in ^{182}W that are smaller than 2 ppm (Fig. S-2; Table S-3).

Supplementary Figures

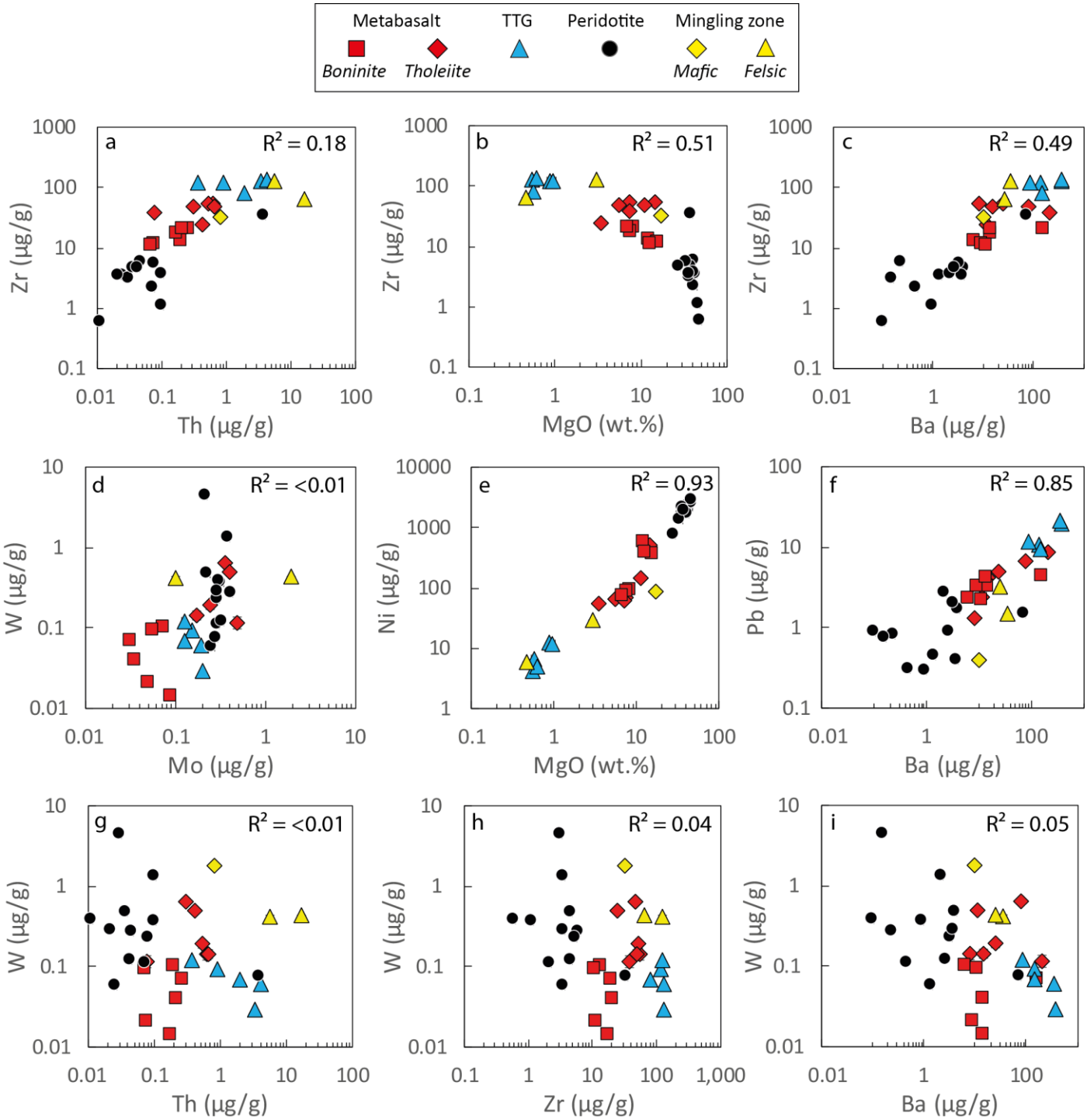

Figure S-1 **(a-f)** Trace element variation diagrams illustrating that our samples exhibit linear co-variations between various compatible and incompatible element concentrations. Most incompatible elements (Zr, Th, Nb, Ba, Pb) show expected enrichments in more differentiated rocks **(a-d, f)**, whereas compatible elements such as Mg, Ni are more depleted **(b, e)**. These differentiation trends are also preserved for some fluid mobile elements such as Ba and Pb **(c-f)**. However, the incompatible and fluid mobile element W shows no co-variation with any other parameter (**g-i**; red squares: Boninitic metabasalts, red diamonds: tholeiitic metabasalts, yellow diamonds: TTGs, black circles: mantle peridotite).

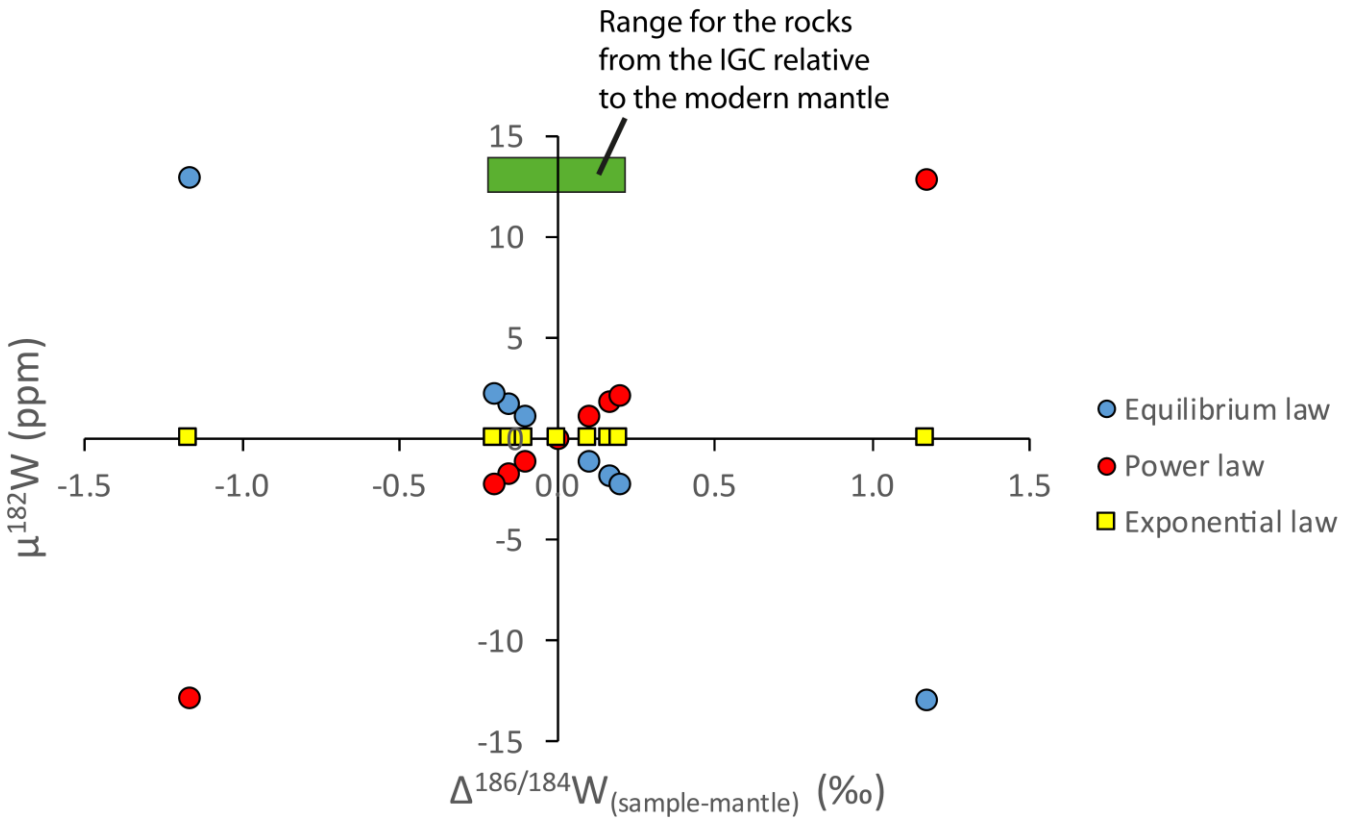

Figure S-2 In most W isotope studies mass dependent isotope fractionation that occurred during the chemical separation of W and the measurement of W isotope abundances is corrected assuming the exponential mass fractionation law. However, natural stable W isotope fractionation prior to the separation and measurement of W isotopes might be better described by another mass fractionation law. This figure shows the apparent excesses/depletions in ^{182}W that is generated by the exponential law although previous natural stable W isotope fractionation followed a different law. The larger the observed range in stable W isotope compositions relative to an unfractionated modern mantle $\delta^{186/184}W$ value of +0.085 ‰ ($\delta^{186/184}W = \delta^{186/184}W_{sample} - \delta^{186/184}W_{modern\ mantle}$), the larger is the relative apparent excess/depletion in ^{182}W ($\mu^{182}W = \{[(^{182}W/^{184}W)_{sample} / (^{182}W/^{184}W)_{SRM\ 3163}] -1\} \times 10^6$, whereby isotope ratios were previously corrected for instrumental mass bias using the exponential law and a given $^{186}W/^{184}W$ of 0.927672; Völkening *et al.*, 1991). The green shaded area indicates the range observed for rocks of the IGC in SW Greenland relative to a modern mantle $\delta^{186/184}W$ of +0.085 ‰. The excesses in $\mu^{182}W$ of around +13 ppm that are observed in rocks of the IGC (Willbold *et al.*, 2011; Rizo *et al.*, 2016; Dale *et al.*, 2017; Tusch *et al.*, 2019) represent no analytical artefacts due to the application of inappropriate mass fractionation laws.

Supplementary Tables

Data Tables S-1 to S-3 are available to download from the online version of this article at http://www.geochemicalperspectivesletters.org/article2024.

Table S-1 Tungsten concentration and stable isotope composition.

Table S-2 Available literature data of the analysed sample set (references below).

Table S-3 Calculation of apparent ^{182}W anomalies due to the application of different mass fractionation laws.

Supplementary Information References

Appel, P.W.U., Rollinson, H.R., Touret, J.L.R. (2001) Remnants of an Early Archaean (> 3.75 Ga) sea-floor, hydrothermal system in the Isua Greenstone Belt. *Precambrian Research* 112, 27–49.

Blichert-Toft, J., Frei, R. (2001) Complex Sm-Nd and Lu-Hf isotope systematics in metamorphic garnets from the Isua supracrustal belt, West Greenland. *Geochimica et Cosmochimica Acta* 65, 3177–3189.

Boyd, A.J. (2018) Geochemical Dynamics of the Isua Supracrustal Belt and the Eoarchean Earth Ph.D. Thesis. University of Copenhagen.

Compston, W., Oversby, V.M. (1969) Lead isotopic analysis using a double spike. *Journal of Geophysical Research* 74, 4338–4348.

Crowley, J.L. (2003) U–Pb geochronology of 3810–3630 Ma granitoid rocks south of the Isua greenstone belt, southern West Greenland. *Precambrian Research* 126, 235–257.

Dale, C.W., Kruijer, T.S., Burton, K.W. (2017) Highly siderophile element and 182W evidence for a partial late veneer in the source of 3.8 Ga rocks from Isua, Greenland. *Earth and Planetary Science Letters* 458, 394–404.

Defant, M.J., Drummond, M.S. (1990) Derivation of some modern arc magmas by melting of young subducted lithosphere. *Nature* 347, 662.

Farquhar, J., Wing, B.A., Mckeegan, K.D., Harris, J.W., Cartigny, P., Thiemens, M.H. (2002) Mass-independent sulfur of inclusions in diamond and sulfur recycling on early Earth. *Science* 298, 2369–2372.

Friend, C., Bennett, V., Nutman A. (2002) Abyssal peridotites> 3,800 Ma from southern West Greenland. *Contributions to Mineralogy and Petrology* 143, 71–92.

Green, D.H. (1976) Experimental testing of" equilibrium" partial melting of peridotite under water-saturated, high-pressure conditions. *The Canadian Mineralogist* 14, 255–268.

Hart, S.R., Zindler, A. (1989) Isotope fractionation laws. *International Journal of Mass Spectrometry and Ion Processes* 89, 287–301.

Hoffmann, J.E., Münker, C., Polat, A., König, S., Mezger, K., Rosing, M.T. (2010) Highly depleted Hadean mantle reservoirs in the sources of early Archean arc-like rocks, Isua supracrustal belt, southern West Greenland. *Geochimica et Cosmochimica Acta* 74, 7236–7260.

Hoffmann, J.E., Münker, C., Næraa, T., Rosing, M.T., Herwartz, D., Garbe-Schönberg, D., Svahnberg, H. (2011) Mechanisms of Archean crust formation inferred from high-precision HFSE systematics in TTGs. *Geochimica et Cosmochimica Acta* 75, 4157–4178.

Hoffmann, J.E., Nagel, T.J., Muenker, C., Næraa, T., Rosing, M.T. (2014) Constraining the process of Eoarchean TTG formation in the Itsaq Gneiss Complex, southern West Greenland. *Earth and Planetary Science Letters* 388, 374–386.

Jenner, F.E., Bennett, V.C., Nutman, A.P., Friend, C.R., Norman, M.D., Yaxley, G. (2009) Evidence for subduction at 3.8 Ga. *Chemical Geology* 261, 83–98.

Kamber, B.S., Moorbath, S. (1998) Initial Pb of the Amıtsoq gneiss revisited. *Chemical Geology* 150, 19–41.

Krabbe, N., Kruijer, T.S., Kleine, T. (2017) Tungsten stable isotope compositions of terrestrial samples and meteorites determined by double spike MC-ICPMS. *Chemical Geology* 450, 135–144.

Kurzweil, F., Münker, C., Tusch, J., Schoenberg, R. (2018) Accurate stable tungsten isotope measurements of natural samples using a 180W-183W double-spike. *Chemical Geology* 476, 407–417.

Kurzweil, F., Münker, C., Grupp, M., Braukmüller, N., Fechtner, L., Christian, M., Hohl, S.V., Schoenberg, R. (2019) The stable tungsten isotope composition of modern igneous reservoirs. *Geochimica et Cosmochimica Acta* 251, 176–191.

Maréchal, C.N., Télouk, P., Albarède, F. (1999) Precise analysis of copper and zinc isotopic compositions by plasma-source mass spectrometry. *Chemical Geology* 156, 251–273.

Moorbath, S., O'nions, R.K., Pankhurst, R.J. (1973) Early Archaean age for the Isua iron formation, West Greenland. *Nature* 245, 138.

Nagel, T.J., Hoffmann, J.E., Münker, C. (2012) Generation of Eoarchean tonalite-trondhjemite-granodiorite series from thickened mafic arc crust. *Geology* 40, 375–378.

Nutman, A.P., Allaart, J.H., Bridgwater, D., Dimroth, E., Rosing M.T. (1984) Stratigraphic and geochemical evidence for the depositional environment of the early Archaean Isua supracrustal belt, southern West Greenland. *Precambrian Research* 25, 365–396.

Nutman, A.P., Mcgregor, V.R., Friend, C.R.L., Bennett, V.C., Kinny, P.D. (1996) The Itsaq gneiss complex of southern West Greenland; the world's most extensive record of early crustal evolution (3900-3600 Ma). *Precambrian Research* 78, 1–39.

Nutman, A.P., Bennett, V.C., Friend, C.R.L., Norman, M.D. (1999) Meta-igneous (non-gneissic) tonalites and quartz-diorites from an extensive ca. 3800 Ma terrain south of the Isua supracrustal belt, southern West Greenland. *Contributions to Mineralogy and Petrology* 137, 364–388.

Nutman, A.P., Friend, C.R.L., Bennett, V.C. (2002) Evidence for 3650–3600 Ma assembly of the northern end of the Itsaq Gneiss Complex, Greenland. *Tectonics* 21.

Nutman, A.P., Friend, C.R.L. (2009) New 1. *Precambrian Research* 172, 189–211.

Polat, A., Hofmann, A.W., Rosing, M.T. (2002) Boninite-like volcanic rocks in the 3.7–3.8 Ga Isua greenstone belt, West Greenland. *Chemical Geology* 184, 231–254.

Polat, A., Hofmann, A.W. (2003) Alteration and geochemical patterns in the 3.7–3.8 Ga Isua greenstone belt, West Greenland. *Precambrian Research* 126, 197–218.

Rapp, R.P., Shimizu, N., Norman, M.D. (2003) Growth of early continental crust by partial melting of eclogite. *Nature* 425, 605.

Rizo, H., Walker, R.J., Carlson, R.W., Touboul, M., Horan, M.F., Puchtel, I.S., Boyet, M., Rosing, M.T. (2016) Early Earth differentiation investigated through 142Nd, 182W, and highly siderophile element abundances in samples from Isua, Greenland. *Geochimica et Cosmochimica Acta* 175, 319–336.

Rose, N.M., Rosing, M.T., Bridgwater, D. (1996) The origin of metacarbonate rocks in the Archaean Isua supracrustal belt, West Greenland. *American Journal of Science* 296, 1004–1044.

Rosing, M.T., Rose, N.M., Bridgwater, D., Thomsen, H.S. (1996) Earliest part of Earth's stratigraphic record. *Geology* 24, 43–46.

Rosing, M.T. (1999) 13C-depleted carbon microparticles in> 3700-Ma sea-floor sedimentary rocks from West Greenland. *Science* 283, 674–676.

Russell, W.A., Papanastassiou, D.A., Tombrello, T.A. (1978) Ca isotope fractionation on the Earth and other solar system materials. *Geochimica et Cosmochimica Acta* 42, 1075–1090.

Smithies, R.H. (2000) The Archaean tonalite–trondhjemite–granodiorite (TTG) series is not an analogue of Cenozoic adakite. *Earth and Planetary Science Letters* 182, 115–125.

Szilas, K., Kelemen, P.B., Rosing, M.T. (2015) The petrogenesis of ultramafic rocks in the> 3.7 Ga Isua supracrustal belt, southern West Greenland. *Gondwana Research* 28, 565–580.

Tatsumi, Y. (1989) Boninites and high-Mg andesites: tectonics and petrogenesis. In: Crawford A.J. (Ed.) *Boninites and related rocks*. Unwin Hypman, London, 50–71.

Tusch, J., Sprung, P., van de Löcht, J., Hoffmann, J.E., Boyd, A.J., Rosing, M.T., Münker, C. (2019) Uniform 182W isotope compositions in Eoarchean rocks from the Isua region, SW Greenland. *Geochimica et Cosmochimica Acta* 257, 284-310.

van de Löcht, J., Hoffmann, J.E., Li, C., Wang, Z., Becker, H., Rosing, M.T., Kleinschrodt, R., Münker, C. (2018) Earth's oldest mantle peridotites show entire record of late accretion. *Geology* 46, 199–202.

van de Löcht, J., Hoffmann, J.E., Rosing, M.T., Sprung, P., Münker, C. (2020) Preservation of Eoarchean mantle processes in ~3.8 Ga peridotite enclaves in the Itsaq Gneiss Complex, southern West Greenland. *Geochimica et Cosmochimica Acta* 280, 1-25.

van der Laan, S.R., Flower, M.F.J., Koster Van Groos, A.F. (1989) Experimental evidence for the origin of boninites: Near-liquidus phase relations to 7.5 kbar. In: Crawford A.J. (Ed.) *Boninites and related rocks*. Unwin Hyman, London, 112-147.

Völkening, J., Köppe, M., Heumann, K.G. (1991) Tungsten isotope ratio determinations by negative thermal ionization mass spectrometry. *International Journal of Mass Spectrometry and Ion Processes* 107, 361–368.

Willbold, M., Elliott, T., Moorbath, S. (2011) The tungsten isotopic composition of the Earth's mantle before the terminal bombardment. *Nature* 477, 195.

Wombacher, F., Rehkämper, M. (2003) Investigation of the mass discrimination of multiple collector ICP-MS using neodymium isotopes and the generalised power law. *Journal of analytical atomic spectrometry* 18, 1371–1375.

Young, E.D., Galy, A., Nagahara, H. (2002) Kinetic and equilibrium mass-dependent isotope fractionation laws in nature and their geochemical and cosmochemical significance. *Geochimica et Cosmochimica Acta* 66, 1095–1104.